EIS Investigation of Zinc Electrodeposition in Basic Media at Low Mass Transfer Rates Induced by a Magnetic Field

ARTICLE *in* THE JOURNAL OF PHYSICAL CHEMISTRY B · DECEMBER 1998

Impact Factor: 3.3 · DOI: 10.1021/jp9835263

7 AUTHORS, INCLUDING:

O. Devos
Université Bordeaux 1
38 PUBLICATIONS **560** CITATIONS
SEE PROFILE

Omar Aaboubi
Université de Reims Champagne-Ardenne
64 PUBLICATIONS **595** CITATIONS
SEE PROFILE

Jean-Paul Chopart
Université de Reims Champagne-Ardenne
104 PUBLICATIONS **813** CITATIONS
SEE PROFILE

EIS Investigation of Zinc Electrodeposition in Basic Media at Low Mass Transfer Rates Induced by a Magnetic Field

Olivier Devos,*,† Omar Aaboubi,† Jean Paul Chopart,† Etienne Merienne,† Alain Olivier,† Claude Gabrielli,‡ and Bernard Tribollet‡

CNRS, EP 120 (Dynamique des Transferts aux Interfaces), UFR Sciences, BP 1039, 51687 Reims Cedex 02, France, and UPR 15 CNRS (Physique des Liquides et Électrochimie), Université Pierre et Marie Curie, Tour 22, 4 Place Jussieu, 75252 Paris Cedex 05, France

Received: August 26, 1998; In Final Form: November 23, 1998

This paper is devoted to the description of magnetic field effects on zinc electrodeposition from basic media. The major effect of the magnetic field stems from a slight magnetohydrodynamic forced convection located close to the cathodic interface. Classical impedance analysis reveals that the reaction mechanism is governed by two diffusing species, Zn(II) and OH^-, the contributions of which have been discerned. This leads to a good agreement between experimental and theoretical impedance diagrams and shows, once again, that the magnetic field exerts no effect upon the transfer kinetics.

Introduction

Because of its industrial use in alkaline batteries, the interface between zinc and highly concentrated basic solutions (7 M KOH) has been widely studied by means of kinetic techniques, regarding zinc electrodeposition as electrodissolution.[1−7] Wiart et al. have notably proposed reaction mechanisms by using electrochemical impedance measurements.[8−12] They have shown that, according to the cathodic potential, several deposit morphologies can be observed. The surface of a deposit grown under a low overvoltage exhibits a spongy aspect and becomes compact at higher overvoltages, while the metal growth under still larger overvoltages is dendritic.[13,14]

Under experimental conditions where mass transport is not the rate-limiting step, the aforementioned authors have proposed a model valid for low overvoltages. A two-step discharge of zincate ions through an oxide-containing layer whose ionic and electronic conductivities and geometrical properties are potential dependent accounts for the current−voltage curve and electrochemical impedances. The growth of a granular deposit is associated with the existence of a uniformly conductive layer on the whole electrode surface. This layer disappears when the overvoltage is shifted cathodically by several millivolts from the equilibrium potential.

To investigate situations where mass transport is the rate-limiting step, it is necessary to analyze conditions where the overvoltage is larger, and we have chosen to work at three-fourths of the diffusion-limiting current. Under this condition, zinc deposits are compact, which gives rise to stationary currents for sufficiently long times.

To demonstrate diffusion limitations, it is necessary to work with a sufficiently high mass transport to overcome the natural convection but sufficiently low not to eliminate its effect. As an example, Wiart et al. worked with a disk electrode rotating at 2500 rpm to completely eliminate mass transport limitations and studied only heterogeneous kinetics. Stable low-rotation velocities of the electrode are not easy to achieve, so we have chosen to use mass transport enhancements induced by magnetic fields on a steady electrode.[15−22] As under the present experimental conditions, a 1 T magnetic field increases mass transport like, about, a 100 rpm rotating electrode, it is easier to explore the equivalent of a few tens of rpm rotation velocities by means of this technique rather than using the rotating electrode.

It was already shown that the stationary limiting current on a steady electrode is proportional to $B^{1/3}C^{4/3}$ where C is the electroactive species concentration and B the magnetic field intensity.[23,24] The ac impedance diagrams plotted in a complex plane are similar to the diffusion impedance diagrams obtained on a nonuniformly accessible electrode, i.e. on an electrode where the thickness of the diffusion layer is not constant over the surface.[24] Another dynamic technique based on the measurement of the magnetohydrodynamical transfer function.[25−27] allowed determination of the diffusion coefficient of zincate at the limiting-current value.[28,29]

Moreover, a previous study on copper electrodeposition in an acidic medium has already shown that magnetic fields increase the electrolytic current when it is mass transport controlled but do not influence charge transfer kinetics.[30,31]

In this paper, we report results on zinc electrodeposition in highly concentrated KOH solutions by means of steady state and dynamic techniques under conditions where this process is mass transport controlled.

Theory

Zinc deposition is supposed to occur mainly from zincate ions $Zn(OH)_4^{2-}$ and to release OH^- ions.[6] Various mechanisms for the discharge of Zn^{2+} ions have been proposed whose details are very complicated and sometimes contradictory. As an example, Bockris et al.[1] have proposed the following mechanism:

$$Zn(OH)_4^{2-} \rightleftarrows Zn(OH)_3^- + OH^-$$

$$Zn(OH)_3^- + e^- \rightleftarrows Zn(OH)_2^- + OH^-$$

$$Zn(OH)_2^- \rightleftarrows ZnOH + OH^-$$

$$ZnOH + e^- \rightleftarrows Zn + OH^- \quad (1)$$

† UFR Sciences.
‡ Université Pierre et Marie Curie.

10.1021/jp9835263 CCC: $18.00
Published on Web 12/31/1998

Sufficiently high overvoltages, where the two-step electron transfer is sufficiently fast to ignore both the Zn(I) concentration change and the anodic current, were investigated. Under these conditions, the total current can be considered to be equal to[32]

$$I_F = nFAk_c C^a_{Zn(II)} C^b_{OH^-} \quad (2)$$

where $C_{Zn(II)}$ and C_{OH^-} are the concentrations of Zn(II) and OH^- respectively and a and b are their reaction orders whose values are under discussion in the literature (Bockris et al.[1] have given $a = 1$ and $b = -1$ as average values from their experimental results). In the absence of an accurate description of the deposition heterogeneous kinetics, it will be formally considered hereafter that the total current formally depends on voltage V and $C_{Zn(II)}$ and C_{OH^-} concentrations.

Therefore, the responses of the faradic current, ΔI_F, and concentrations, $\Delta C_{Zn(II)}$ and ΔC_{OH^-}, to a small amplitude potential perturbation, ΔV, are related by

$$\Delta I_F = \left(\frac{\partial I_F}{\partial C_{Zn(II)}}\right)_{C_{OH^-},V} (\Delta C_{Zn(II)})_{y=0} + \left(\frac{\partial I_F}{\partial C_{OH^-}}\right)_{C_{Zn(II)},V} (\Delta C_{OH^-})_{y=0} + \left(\frac{\partial I_F}{\partial V}\right)_{C_{Zn(II)},C_{OH^-}} \Delta V \quad (3)$$

when

$$\left(\frac{\partial I_F}{\partial V}\right)_{C_{Zn(II)},C_{OH^-}} = \frac{1}{R_{ct}} \quad (4)$$

defines the charge transfer resistance, $1/R_{ct}$.

Then, the faradic impedance Z_F is defined by

$$Z_F = \frac{\Delta V}{\Delta I_F} \quad (5)$$

$$Z_F = R_{ct}\left[1 - \left(\frac{\partial I_F}{\partial C_{Zn(II)}}\right)_{C_{OH^-},V}\left(\frac{\Delta C_{Zn(II)}}{\Delta I_F}\right)_{y=0} - \left(\frac{\partial I_F}{\partial C_{OH^-}}\right)_{C_{Zn(II)},V}\left(\frac{\Delta C_{OH^-}}{\Delta I_F}\right)_{y=0}\right] \quad (6)$$

The diffusion impedance, Z_D, can be defined as

$$Z_D = -R_{ct}\left(\frac{\partial I_F}{\partial C_{Zn(II)}}\right)_{C_{OH^-},V}\left(\frac{\Delta C_{Zn(II)}}{\Delta I_F}\right)_{y=0} - R_{ct}\left(\frac{\partial I_F}{\partial C_{OH^-}}\right)_{C_{Zn(II)},V}\left(\frac{\Delta C_{OH^-}}{\Delta I_F}\right)_{y=0} \quad (7)$$

where

$$Z_F = R_{ct} + Z_D \quad (8)$$

$\Delta C_{Zn(II)}$ and ΔC_{OH^-} are solutions of the convective diffusion equations applied in the case of a laminar flow along a horizontal circular electrode

$$j\omega\Delta C_i - D_i\frac{\partial^2 \Delta C_i}{\partial y^2} + \alpha y\frac{\partial \Delta C_i}{\partial x} = 0 \qquad i = Zn(II), OH^- \quad (9)$$

where x is the radial axis and y the perpendicular axis relative to the electrode surface.

α is the velocity gradient of the fluid on the electrode surface which is proportional to B.[24]

$$\alpha \propto B \quad (10)$$

together with the following boundary conditions:

at $y = 0$:

$$\frac{\Delta I_F}{nFA} = -D_{Zn(II)}\left(\frac{\partial \Delta C_{Zn(II)}}{\partial y}\right)_{y=0} = D_{OH^-}\left(\frac{\partial \Delta C_{OH^-}}{\partial y}\right)_{y=0} \quad (11)$$

Therefore, from eq 11

$$Z_D = \left(\frac{\partial I_F}{\partial C_{Zn(II)}}\right)_{C_{OH^-},V}\frac{R_{ct}}{2FAD_{Zn(II)}}\left[\frac{\Delta C_{Zn(II)}}{(\partial \Delta C_{Zn(II)}/\partial y)}\right]_{y=0} - \left(\frac{\partial I_F}{\partial C_{OH^-}}\right)_{C_{Zn(II)},V}\frac{R_{ct}}{2FAD_{OH^-}}\left[\frac{\Delta C_{OH^-}}{(\partial \Delta C_{OH^-}/\partial y)}\right]_{y=0} \quad (12)$$

In eq 12, both $[\Delta C_{Zn(II)}/(\partial \Delta C_{Zn(II)}/\partial y)]_{y=0}$ and $[\Delta C_{OH^-}/(\partial \Delta C_{OH^-}/\partial y)]_{y=0}$ terms are obtained from the resolution of eq 9,[24,27] i.e.

$$\left[\frac{\Delta C_i}{(\partial \Delta C_i/\partial y)}\right]_{y=0} = \left(\frac{D_i}{\alpha d^5}\right)^{1/3}\frac{1}{H(\sigma_i)} \quad (13)$$

where $H(\sigma_i)$ is a hydrodynamic transfer function depending on the dimensionless frequency, σ_i, defined by

$$\sigma_i = \omega(d^2/D_i\alpha^2)^{1/3} \quad (14)$$

i.e.

$$\sigma_i \propto \frac{\delta_i^2}{D_i} \quad (15)$$

The total convective diffusion impedance is equal to the sum of the partial diffusion impedances $Z_{D_{Zn(II)}}$ and $Z_{D_{OH^-}}$, which are equal to

$$Z_D = R_{ct}\kappa_{Zn(II)}\frac{1}{H(\sigma_{Zn(II)})} + R_{ct}\kappa_{OH^-}\frac{1}{H(\sigma_{OH^-})} \quad (16)$$

where

$$\kappa_i = \frac{\chi_i}{(\alpha D_i^2 d^5)^{1/3}} \qquad i = Zn(II), OH^- \quad (17)$$

and χ_i are quantities which contain the parameters of zinc deposition kinetics, e.g.

$$\chi_i = \frac{1}{2FA}\left(\frac{\partial I_F}{\partial C_i}\right)_{C_{j\neq i}V} \quad (18)$$

The transfer function, $H(\sigma_i)$, is defined for each of the two diffusing species by the following expressions"[33]

for $\sigma_i \leq 4$

$$|H(\sigma_i)| = H(0)\{1 + 0.339\sigma_i^2 - 0.0058\sigma_i^4\}^{1/2}$$

$$\phi_i = -\arctan\{0.48567\sigma_i(1 - 0.06\sigma_i^2 + 0.0018\sigma_i^4)\} \quad (19)$$

for $\sigma_i > 4$

$$|H(\sigma_i)| = H(0)\{0.865/\sigma_i^{1/2}(1 + 0.225/\sigma_i^{3/2})\}^{-1}$$

$$\phi_i = -\arctan\{1 - 0.45/\sigma_i^{3/2}\} \quad (20)$$

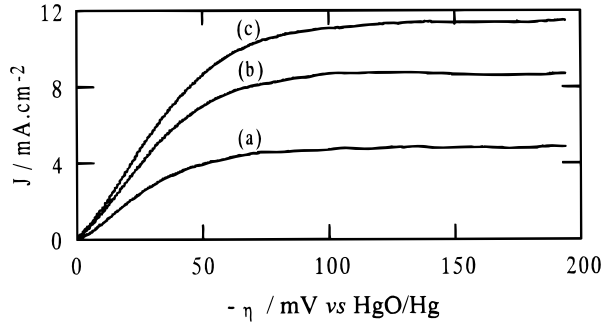

Figure 1. Experimental current−voltage curves for the $Zn(OH)_4^{2-}$/Zn system plotted for various magnetic fields: (a) $B = 0$; (b) $B = 0.3$ T; (c) $B = 0.6$ T. [Zn(II)] = 0.2 M; [KOH] = 7 M; $\upsilon = 20$ mV·min^{-1}.

where $|H(\sigma_i)|$ is the modulus of the hydrodynamic transfer function of species i, ϕ_i is the phase of the transfer function of species i, and $H(0) = 0.8075$.

Experimental Section

The 100 cm^3 three-electrode electrochemical cell was a classical double-jacketed glass beaker where the solution was maintained at 30 °C. The working electrode was a 5 mm diameter zinc disk horizontally located facing downward. The counter electrode was a large-surface zinc-soluble anode located at the bottom of the cell. The reference electrode was a HgO/Hg/KOH (5 M) (Tacussel) electrode. The three electrodes were connected to an electrochemical interface (Solartron 1286). The electrochemical impedance measurements were carried out by means of a frequency response analyzer (Solartron 1250).

The electrolytic solution was prepared by dissolving ZnO (Merck) and KOH in permuted water. A 7 M KOH concentration and various ZnO concentrations were used. The solution was deaerated during 30 min before each experiment.

The whole electrochemical cell was inserted between the pole pieces of an electromagnet (Drusch EAM 20G) which generated a homogeneous magnetic field up to 1 T. The 20 cm diameter pole pieces were cooled by means of water circulation. The magnetic field vector was applied parallelly to the surface of the working electrode. Before each experiment, the electrode surface was polished with abrasive paper (Struers) of grades 1000 and then 4000. The surface was then polished on felt with alumina (grain size 1 μm). After polishing, zinc was deposited, without a magnetic field, at a current equal to three-fourths of the diffusion-limiting current.

In a first step, current−voltage curves were recorded for different values of the magnetic field (Figure 1). As already shown,[24] the diffusion-limiting current increased with B. It was then plotted against $B^{1/3}$ (Figure 2), and a linear relationship was found for magnetic fields higher than 0.12 T. Below, the natural convection biased the current. Therefore, the useful magnetic induction change was chosen between 0.12 and 1 T to investigate mass transport limitations of the zinc deposition process.

Electrochemical impedances were measured at a potential corresponding to three-fourths of the diffusion-limiting current and were plotted in the complex plane [Re(Z_F), −Im(Z_F)] for various intensities of the magnetic field (Figure 3). The impedance diagrams present two characteristic parts, each of them changing with the magnetic field. The high-frequency part characterizes charge transfer processes in parallel with double-layer charging. In a forthcoming paper, the influence of magnetic fields on heterogeneous kinetics will be analyzed. The low-frequency loop with a 45° start characterizes the diffusion process. Compared to the work of Wiart et al., it is obvious that the analyzed overvoltages were sufficiently high to ignore the Zn(I) relaxation, as there is no intermediate loop between these two features.

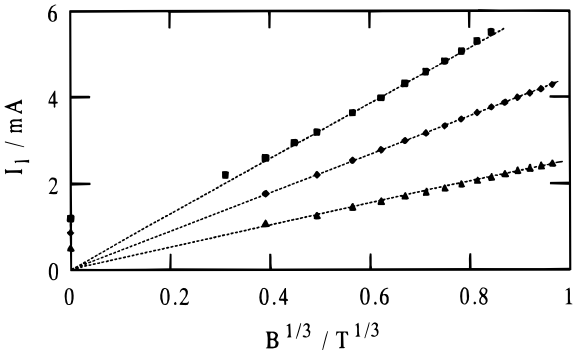

Figure 2. Cathodic limiting current vs $B^{1/3}$: (▲) [Zn(II)] = 0.1 M; (◆) [Zn(II)] = 0.15 M; (■) [Zn(II)] = 0.2 M. [KOH] = 7 M.

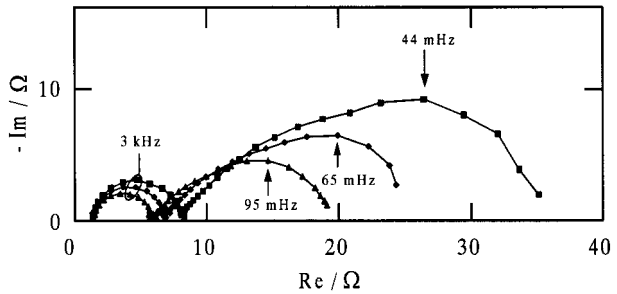

Figure 3. Electrochemical impedances in the Nyquist plane for various magnetic field intensities: (■) $B = 0.3$ T; (◆) $B = 0.6$ T; (▲) $B = 0.9$ T. [Zn(II)] = 0.2 M; [KOH] = 7 M; $\eta = -70$ mV.

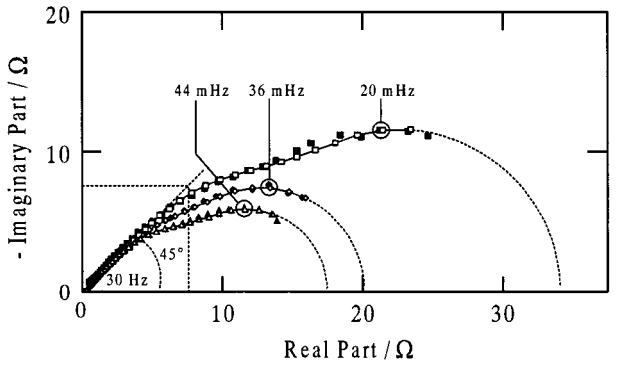

Figure 4. Experimental and calculated (from eq 16) diffusion-convective impedances in the Nyquist plane for various magnetic field intensities. $(dV/dI)_{exp}$: (■) $B = 0.3$ T; (◆) $B = 0.6$ T; (▲) $B = 0.75$ T. $(dV/dI)_{cal}$: (□) $B = 0.3$ T; (◇) $B = 0.6$ T; (△) $B = 0.75$ T. [Zn(II)] = 0.15 M; [KOH] = 7 M; $\eta = -65$ mV.

Figure 4 shows the experimental impedance diagrams from which the resistance $R_{ct} + R_s$ was substracted (where R_s is the electrolyte resistance). They reveal a decrease of the amplitude of the diffusion impedance when magnetic field intensity increased. In addition, the real low-frequency limit was attained at frequencies as much higher as the magnetic field increased. These results are in good agreement with those obtained for a reversible electrochemical system like potassium ferri−ferrocyanide.[24,26] The tangential convection generated by the magnetic field in the close vicinity of the working electrode affects the diffusion loop in the same way as the convection generated by a rotating electrode.[34,35] However, under the present experimental conditions, the convective regime generated by a magnetic field is much lower than the one generated by a rotating electrode; in fact, the increase of the mass transport

TABLE 1: Values for the Coefficients of Eq 16 Calculated with the Matrix-Fitting Software for Various Magnetic Field Intensities[a]

	B/*T*					
	0.15	0.3	0.45	0.6	0.75	0.9
R_{ct}/Ω	7.6	5.9	4.6	4.8	4.1	4.0
$\kappa_{Zn(II)}B^{1/3}$/MKSA u	0.23	0.23	0.25	0.24	0.23	0.22
$\kappa_{OH^-}B^{1/3}$/MKSA u	0.052	0.069	0.067	0.067	0.054	0.057
$\delta_{Zn(II)}D_{Zn(II)}^{-1/2}/s^{1/2}$	3.45	2.39	2.09	1.91	1.81	1.62
$\delta_{OH^-}D_{OH^-}^{-1/2}/s^{1/2}$	1.32	0.92	0.75	0.73	0.69	0.65
$R_{ct}I$/mV	27	28	26	28	27	27

[a] [Zn(II)] = 0.2 M; [KOH] = 7 M; $\eta = -70$ mV.

controlled current, generated by a 1 T magnetic field, corresponds to a rotation velocity lower than 100 rpm of a rotating electrode.

The use of a rotating disk electrode for controlling a mass transport rate sufficiently low to be limiting for the investigated process is quite difficult because it needs a very high resolution for changing the rotation velocity. Generally, the useful rotation velocities are higher than 100 rpm. If mass transport influence has to be eliminated, it is usually sufficient to rotate at 2000 rpm in order to impose a forced convection which sufficiently accelerates mass transport in a way that heterogeneous kinetics can be the rate-determining step. Hence, the slighter convection generated by a magnetic field is particularly adapted to the control of mass transport for zinc deposition.

Discussion

A detailed analysis of the diffusion loops (Figure 4) obtained for various values of the magnetic field reveals two diffusional impedances with different time constants. Zincate species diffuse from the solution bulk toward the working electrode to be reduced. During reduction, OH^- species are produced and then diffuse from the working electrode toward the bulk solution. Therefore, two diffusing species $Zn(OH)_4^{2-}$ (i.e., Zn(II)) and OH^- contribute to the total diffusion impedance with very different diffusion coefficients ($D_{Zn(OH)_4^{2-}} \ll D_{OH^-}$).

A home made matrix-fitting technique allows the five characteristic parameters of eq 16 to be determined from the experimental impedances ($R_{ct} + R_s$), $\kappa_{Zn(II)}$, κ_{OH^-}, $\delta_{Zn(II)}^2/D_{Zn(II)}$, and $\delta_{OH^-}^{-2}/D_{OH^-}$.

These parameters are listed in Table 1 for various values of the magnetic field intensity. The diagrams, calculated with the fitting software by using the experimental parameters, are practically identical, frequency for frequency, to the experimental diagrams for the tested magnetic field intensities. In addition, the knowledge of the parameter values allows the impedance diagrams to be extrapolated down to the lowest frequencies represented by dashed lines in Figure 4.

The values listed in Table 1 show that the convective regime generated by the magnetic field decreases the thickness of the diffusion layer for each species, in agreement with theoretical predictions. The thickness of the two diffusion layers are proportional to $B^{-1/3}$, which results from the hydrodynamic control on the diffusion of the two species by the magnetic field (Figure 5).[24,27] Because the gradient of the fluid velocity, α, is proportional to *B*, at constant overvoltage, the plots of $\kappa_{Zn(II)}B^{1/3}$ and $\kappa_{OH^-}B^{1/3}$ are constants for the entire magnetic field range studied, as demonstrated in Figure 6. This result shows the *B* independence of the kinetic parameters for this electrochemical system, confirming previous results[30,31] on Cu electrodeposition in an H_2SO_4 medium.

Figure 7 shows the experimental impedance plotted in a Bode plane. The plotting against the partial reduced frequency $f^+ = fB^{-2/3}$ (eqs 10 and 14) shows that all the diagrams are superposed in the whole frequency domain. As the reduced frequency is magnetic field dependent, the control of the transport of the two diffusing species by this quantity is confirmed. The full line curve represents the mean of the impedances calculated

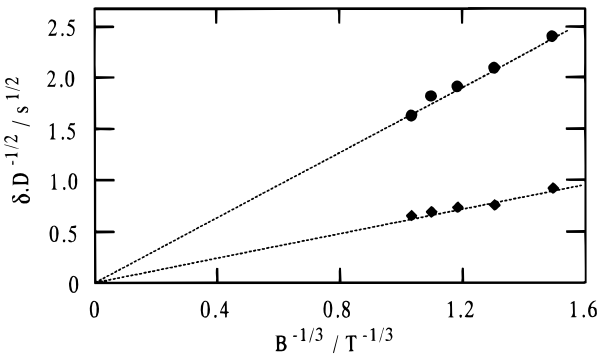

Figure 5. $\delta_{Zn(II)}D_{Zn(II)}^{-1/2}$ (●) and $\delta_{OH^-}D_{OH^-}^{-1/2}$ (◆) values calculated with the matrix-fitting software vs $B^{-1/3}$. [Zn(II)] = 0.2 M; [KOH] = 7 M; $\eta = -70$ mV.

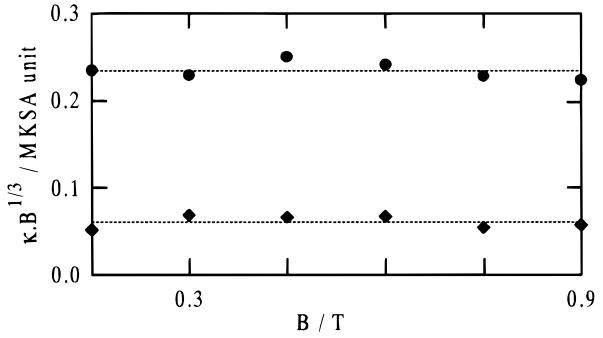

Figure 6. $\kappa_{Zn(II)}B^{1/3}$ (●) and $\kappa_{OH^-}B^{1/3}$ (◆) values calculated with the matrix-fitting software vs *B*. [Zn(II)] = 0.2 M; [KOH] = 7 M; $\eta = -70$ mV.

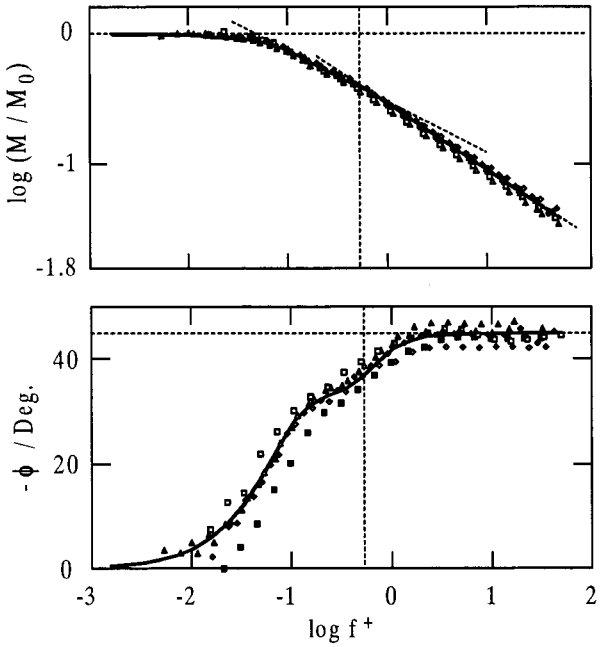

Figure 7. Experimental and calculated diffusion-convective impedances in the Bode plane vs log f^+ for various magnetic field intensities: (□) $B = 0.15$ T; (■) $B = 0.3$ T; (◇) $B = 0.45$ T; (◆) $B = 0.6$ T; (△) $B = 0.75$ T; (▲) $B = 0.9$ T. Solid line: impedance calculated from eq 16. [Zn(II)] = 0.2 M; [KOH] = 7 M; $\eta = -70$ mV.

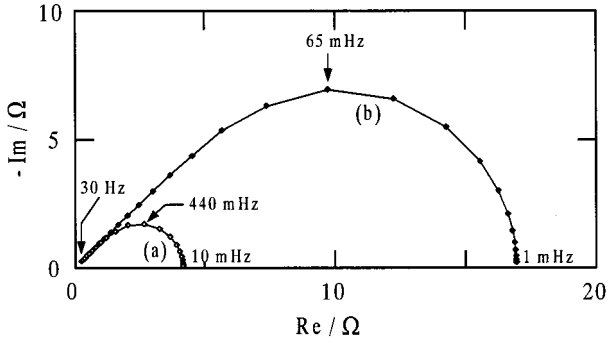

Figure 8. Calculated diffusion-convective impedances of the zincate ion (◆) and the hydroxide ion (◇) in the Nyquist plane. [Zn(II)] = 0.2 M; [KOH] = 7 M; B = 0.45 T; η = −70 mV.

TABLE 2: Diffusion Resistance Values for Various Magnetic Field Intensities[a]

	B/T					
	0.15	0.3	0.45	0.6	0.75	0.9
$R_{D_{Zn(II)}}/\Omega$	32.5	20.8	16.5	14.8	11.5	10.5
$R_{D_{OH^-}}/\Omega$	7.2	6.2	4.4	4.1	2.7	2.7
$R_{D_{calc}}/\Omega$	39.8	27.0	20.9	19.0	14.3	13.1
$R_{D_{exp}}/\Omega$	37.0	29.0	22.2	19.0	15.0	13.5

[a] [Zn(II)] = 0.2 M; [KOH] = 7 M; η = −70 mV.

with eq 16 from the experimental impedances for various values of the magnetic field. The experimental diagrams are in good agreement with theory. In addition, the existence of two diffusional impedances is clearly shown by the steep change of the modulus slope at a reduced frequency equal to, about, 0.63 Hz·T$^{-2/3}$ and by the still neater steep change of the phase at the same reduced frequency.

By using the values of the parameters of each diffusion impedance, the latter can be separately calculated. Figure 8 shows the two diffusion impedances relative to Zn(II) and OH^-, respectively, obtained for a 0.45 T magnetic field. The diffusion impedance relative to OH^- changes for frequencies ranging from 30 Hz to 10 mHz. The diffusion impedance relative to Zn(II), which is very much larger, decreases to 1 mHz. The maximum of the imaginary part appears at 440 mHz for OH^- and 65 mHz for Zn(II). These features explain the steep changes of the slope of the experimental diagrams observed in the Bode plane (Figure 7) and the bump observed in the complex plane plot (Figure 4).

The diffusion resistances, R_{D_i}, are defined at the low-frequency limit of the diffusion impedances as follows:

$$\omega \rightarrow 0: \quad Z_{D_i} = R_{D_i} \qquad i = Zn(II), OH^- \tag{21}$$

$R_{D_{Zn(II)}}$ and $R_{D_{OH^-}}$ were calculated for various values of the magnetic field by using eqs 22 and 23 and are listed in Table 2.

$$R_{D_{Zn(II)}} = H(0)\frac{R_{ct}\chi_{Zn(II)}}{(\alpha D_{Zn(II)}{}^2 d^5)^{1/3}} = H(0)\, R_{ct}\kappa_{Zn(II)} \tag{22}$$

$$R_{D_{OH^-}} = H(0)\frac{R_{ct}\chi_{OH^-}}{(\alpha D_{OH^-}{}^2 d^5)^{1/3}} = H(0)\, R_{ct}\kappa_{OH^-} \tag{23}$$

R_{ct}, $\kappa_{Zn(II)}$, and κ_{OH^-} values were obtained by the matrix-fitting technique. In agreement with a previous study of the $K_3Fe(CN)_6/K_4Fe(CN)_6$ system,[26,27] $R_{D_{Zn(II)}}$ and $R_{D_{OH^-}}$ decrease when B increases.

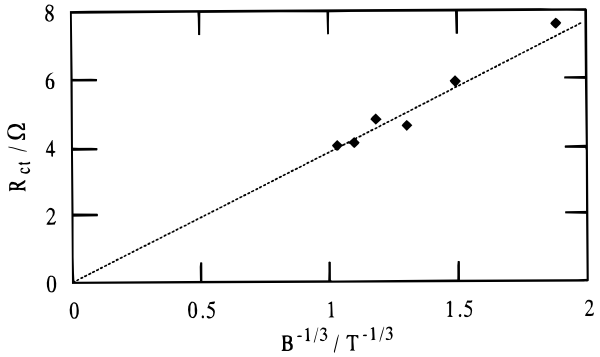

Figure 9. Charge transfer resistance calculated with the matrix-fitting software vs $B^{-1/3}$. [Zn(II)] = 0.2 M; [KOH] = 7 M; η = −70 mV.

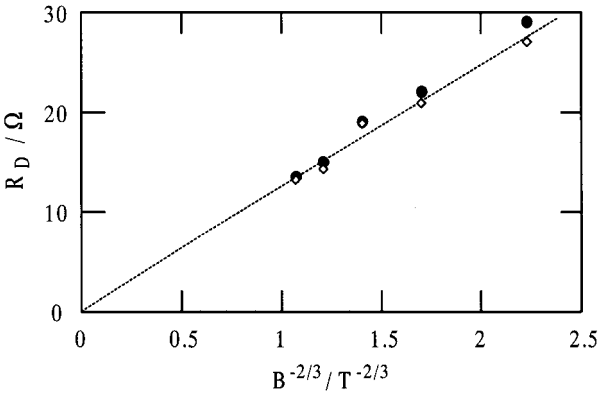

Figure 10. $R_{D_{exp}}$ (◇) and $R_{D_{cal}}$ (●) vs $B^{-2/3}$. [Zn(II)] = 0.2 M; [KOH] = 7 M; η = −70 mV.

The low-frequency limit of the total convective diffusion impedance is equal to

$$R_{D_{cal}} = R_{D_{OH^-}} + R_{D_{Zn(II)}} \tag{24}$$

The calculated, $R_{D_{cal}}$, and experimental, $R_{D_{exp}}$, total diffusion impedances are listed in Table 2 for various values of B and show a good agreement between theory and experiment.

From Table 1, it is obvious that, at constant polarization, the $R_{ct}I$ product is practically constant in the studied magnetic field range, which shows that the magnetic field does not influence the kinetics of the electrode charge transfer. Figure 9 shows the plot of R_{ct} against $B^{-1/3}$.

As the mass transport controlled electrodeposition current generated by a magnetic field is proportional to $B^{1/3}$, it is not surprising that the R_{ct} vs $B^{-1/3}$ plot follows a straight line crossing the origin. In addition, as the fluid velocity gradient, α, is proportional to B, from eqs 22−24, R_D is proportional to $B^{-2/3}$. This feature is fully verified in Figure 10, where $R_{D_{cal}}$ and $R_{D_{exp}}$ are plotted against $B^{-2/3}$.

In the potential range corresponding to three-fourths of the diffusion-limiting current (about 70 mV), the contribution of adsorbed intermediate species may be neglected, and by taking into account the double-layer capacity, C_d, we derive the global electrochemical impedance:

$$Z_F = R_s + \frac{R_{ct} + Z_{D_{OH^-}} + Z_{D_{Zn(II)}}}{1 + jC_d\omega(R_{ct} + Z_{D_{OH^-}} + Z_{D_{Zn(II)}})} \tag{25}$$

Figure 11 shows that the impedances calculated from the values of the parameter-fitting software superimpose frequency by frequency on the experimental impedances in the entire frequency domain studied here. The influence of the magnetic

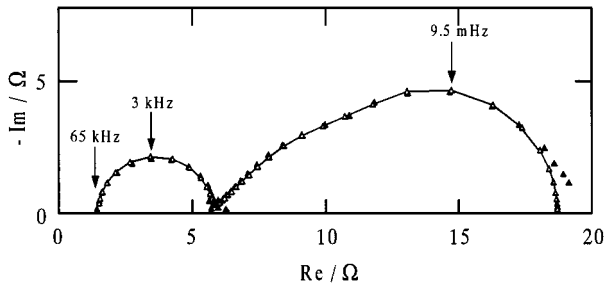

Figure 11. Electrochemical impedances in the Nyquist plane: (▲) experimental impedance, [Zn(II)] = 0.2 M, [KOH] = 7 M, $B = 0.9$ T; (△) impedance calculated from eq 25.

field on the high-frequency capacitive loop, which characterizes the charge transfer kinetics at the electrode, will be discussed in a future paper.

Conclusion

By using impedance techniques, it was shown that, under experimental conditions where the electrodeposition current of zinc in a basic medium was mass transport controlled, the diffusion of two species occurred. Zincate ions came from the solution to be reduced and hydroxide ions were released and left the electrode surface. This investigation was possible because of the accurate control of the hydrodynamical regime generated by a magnetic field under low mass transfer control conditions. Diard showed that it was quite possible to observe theoretically two diffusion loops by an EIS investigation of a quasi-reversible system with both anodic and cathodic current contributions and with two different diffusion coefficients for the Ox and Red species.[36] In this paper, we showed experimentally the existence of two diffusion processes if we consider only the cathodic current contribution. Moreover, the investigation of the diffusional response allowed us to show that magnetic fields less intense than 1 T did not influence the charge transfer kinetics.

Nomenclature

A	electrode surface (m^2)
a, b	reaction order of $Zn(OH)_4^{2-}$ and OH^- species
B	magnetic field (T)
C_d	double-layer capacitance ($mF \cdot cm^{-2}$)
C_i	electrode surface concentration of species i ($mol \cdot m^{-3}$)
D_i	diffusion coefficient of species i ($m^2 \cdot s^{-1}$)
d	electrode diameter (m)
f	frequency (Hz)
f^+	partial reduced frequency
$H(\sigma_i)$	hydrodynamic transfer function of species i
I_F	faradic electrolysis current (A)
J	current density ($A \cdot m^{-2}$)
j	$(-1)^{1/2}$
k_c	cathodic kinetic constant ($m \cdot s^{-1}$)
M	modulus of the electrochemical impedance
M_0	modulus of the electrochemical impedance at low-frequency range
n	number of electrons exchanged during the reaction
R_s	solution resistance (Ω)
R_{ct}	charge transfer resistance (Ω)
R_{D_i}	diffusion resistance of species i (Ω)
V	potential (V)
x, y, z	spacial axes (m)
Z_{D_i}	diffusion impedance of species i (Ω)
Z_F	Faradic impedance (Ω)

Greek Characters

α	velocity gradient (s^{-1})
χ_i	coefficient depending on kinetic parameters (MKSA u)
δ_i	thickness of the diffusion layer of species i (m)
ϕ	phase (rad)
η	overpotential (V)
σ_i	dimensionless frequency
ω	pulsation ($rad \cdot s^{-1}$)

References and Notes

(1) Bockris, J. O.; Nagy, Z.; Damjanovic, A. *J. Electrochem. Soc.* **1972**, *19*, 285.
(2) Despic, A. R.; Jovanovic, D.; Rakic, T. *Electrochim. Acta* **1976**, *21*, 63.
(3) Hendrikx, J.; van der Putten, A.; Visscher, W.; Barendrecht, E. *Electrochim. Acta* **1984**, *29*, 81.
(4) Hendrikx, J.; Visscher, W.; Barendrecht, E. *Electrochim. Acta* **1985**, *30*, 999.
(5) Chang, Y. C.; Prentice, G. *J. Electrochem. Soc.* **1984**, *131*, 1466.
(6) Chang, Y. C.; Prentice, G. *J. Electrochem. Soc.* **1985**, *132*, 375.
(7) Baugh, L. M.; Higginson, A. *Electrochim. Acta* **1985**, *30*, 1163.
(8) Epelboin, I.; Ksouri, M.; Wiart, R. *J. Electrochem. Soc.* **1975**, *122*, 1206.
(9) Cachet, C.; Ströder, U.; Wiart, R. *Electrochim. Acta* **1982**, *27*, 903.
(10) Cachet, C.; Saïdani, B.; Wiart, R. *Electrochim. Acta* **1988**, *33*, 405.
(11) Cachet, C.; Saïdani, B.; Wiart, R. *J. Electrochem. Soc.* **1991**, *138*, 679.
(12) Cachet, C.; Saïdani, B.; Wiart, R. *J. Electrochem. Soc.* **1992**, *139*, 644.
(13) Epelboin, I.; Ksouri, M.; Wiart, R. *Faraday Symp. Chem. Soc.* **1978**, *12*, 115.
(14) Froment, M.; Maurin, G. *Electrodeposition Surf. Treat.* **1975**, *3*, 245.
(15) Tacken, R. A.; Janssen, L. J. J. *J. Appl. Electrochem.* **1995**, *25*, 1.
(16) Iwakura, C.; Edamoto, T.; Tamura, H. *Denki Kagaku* **1984**, *52*, 654.
(17) Mohanta, S.; Fahidy, T. Z. *Electrochim. Acta* **1976**, *21*, 149.
(18) Olivier, A.; Chopart, J. P.; Douglade, J.; Gabrielli, C. *J. Electroanal. Chem.* **1987**, *217*, 443.
(19) Lee, J.; Ragsdale, S. R.; Gao, X.; White, H. S. *J. Electroanal. Chem.* **1997**, *422*, 169.
(20) Mori, S.; Satoh, K.; Tanimoto, A. *Electrochim. Acta* **1994**, *39*, 2789.
(21) Leventis, N.; Chen, M.; Gao, X.; Canalas, M.; Zhang, P. *J. Phys. Chem. B* **1998**, *102*, 3512.
(22) Aogaki, R.; Fueki, K.; Makaido, T. *Denki Kagaku* **1976**, *44*, 89.
(23) Aogaki, R.; Fueki, K.; Makaido, T. *Denki Kagaku*, **1975**, 43, 509.
(24) Aaboubi, O.; Chopart, J. P.; Douglade, J.; Olivier, A.; Gabrielli, C.; Tribollet, B. *J. Electrochem. Soc.* **1990**, *137*, 1796.
(25) Olivier, A.; Chopart, J. P.; Douglade, J.; Gabrielli, C.; Tribollet, B. *J. Electroanal. Chem.* **1987**, *227*, 275.
(26) Devos, O.; Aaboubi, O.; Chopart, J. P.; Merienne, E.; Olivier, A.; Gabrielli, C.; Tribollet, B. *Polish J. Chem.* **1997**, *71*, 1160.
(27) Aaboubi, O. Thesis, University of Reims, France, 1991.
(28) Devos, O.; Aaboubi, O.; Chopart, J. P.; Gabrielli, C.; Merienne, E.; Olivier, A.; Tribollet, B. *Proc.—Electrochem. Soc.* **1998**, *97-27*, 164.
(29) Devos, O. Thesis, University of Reims, France, 1997.
(30) Chopart, J. P.; Douglade, J.; Fricoteaux, P.; Olivier, A. *Electrochim. Acta* **1991**, *36*, 459.
(31) Fricoteaux, P.; Olivier, A.; Delmas, R. *J. Electrochem. Soc.* **1992**, *139*, 1096.
(32) Dirkse, T. P. *J. Electrochem. Soc.* **1979**, *126*, 541.
(33) Deslouis, C.; Tribollet, B.; Vorotyntsev, M. A. *J. Electrochem. Soc.* **1991**, *138*, 2651.
(34) Deslouis, C.; Epelboin, I.; Keddam, M.; Lestrade, J. C. *J. Electroanal. Chem.* **1970**, *28*, 57.
(35) Durliat, H.; Delorme, P.; Comtat, M. *Electrochim. Acta* **1985**, *30*, 1071.
(36) Diard, J. P.; Le Gorrec, B.; Montella, C. *Cinétique électrochimique*; Hermann: Paris, 1996.